J Solid State Electrochem (2012) 16:17–24
DOI 10.1007/s10008-010-1269-4

ORIGINAL PAPER

Preparation and characterization of high-rate and long-cycle $LiFePO_4$/C nanocomposite as cathode material for lithium-ion battery

Xingchao Wang · Yudai Huang · Dianzeng Jia · Zaiping Guo · Duo Ni · Ming Miao

Received: 13 June 2010 / Revised: 26 November 2010 / Accepted: 2 December 2010 / Published online: 22 December 2010

Abstract Olivine $LiFePO_4$/C nanocomposite cathode materials with small-sized particles and a unique electrochemical performance were successfully prepared by a simple solid-state reaction using oxalic acid and citric acid as the chelating reagent and carbon source. The structure and electrochemical properties of the samples were investigated. The results show that $LiFePO_4$/C nanocomposite with oxalic acid (oxalic acid: Fe^{2+}=0.75:1) and a small quantity of citric acid are single phase and deliver initial discharge capacity of 122.1 mAh/g at 1 C with little capacity loss up to 500 cycles at room temperature. The rate capability and cyclability are also outstanding at elevated temperature. When charged/discharged at 60 °C, this materials present excellent initial discharge capacity of 148.8 mAh/g at 1 C, 128.6 mAh/g at 5 C, and 115.0 mAh/g at 10 C, respectively. The extraordinarily high performance of $LiFePO_4$/C cathode materials can be exploited suitably for practical lithium-ion batteries.

Keywords $LiFePO_4$/C nanocomposites · High-rate · Long-cycle · Cathode materials · Lithium-ion battery

X. Wang · Y. Huang · D. Jia (✉)
Institute of Applied Chemistry, Xinjiang University,
Urumqi 830046, People's Republic of China
e-mail: jdz0991@gmail.com

Z. Guo
School of Mechanical, Materials and Mechatronic Engineering,
University of Wollongong,
Wollongong NSW 2522, Australia

D. Ni · M. Miao
Xinjiang Cancer Institute & Hospital,
Urumqi 830000, People's Republic of China

Introduction

Rechargeable lithium-ion batteries are becoming more popular with the increasing demands for electric vehicles and other portable devices [1, 2]. They are able to deliver high-energy densities and have longer operational lifetimes than many other battery systems [3]. Olivine structure lithium iron phosphate ($LiFePO_4$), as cathode material for lithium-ion batteries, has attracted intensive studies since 1997 [4]. $LiFePO_4$ material is considered to be a state-of-the-art lithium-ion battery cathode material to substitute for toxic and expensive $LiCoO_2$, due to its lack of toxicity, low cost, high safety, superior thermal stability, and environmental friendliness [5]. In addition, $LiFePO_4$ has high theoretical capacity (170 mAh/g) and better cycling stability, with a flat voltage profile of about 3.4 V versus Li/Li^+ [6].

However, there are two major impediments to the commercial application of $LiFePO_4$: one is the low electronic conductivity (10^{-7}–10^{-9} S/cm), which leads to its poor rate capability; the other is the slow lithium-ion diffusion across the $LiFePO_4/FePO_4$ boundary [4, 7]. To eliminate the two major impediments of $LiFePO_4$, numerous approaches such as conductive additive coating [8–10], supervalence cation doping [11, 12], and minimizing particle size by different synthesis routes [13–15], have been reported. The synthesis method to produce $LiFePO_4$ has been an important factor for its large-scale commercial manufacture. Various synthesis routes have been proposed to prepare $LiFePO_4$, such as solid-state reaction [16–18], sol–gel preparation [19, 20], co-precipitation [21, 22], microwave processes [23, 24], hydrothermal reaction [25–27], carbothermal reduction method [28, 29], vapor deposition procedure [30], etc. Compared to other methods, solid-state reaction route can meet the needs of large-scale

commercial manufacture [31]. However, larger particles and low electrochemical performance are obstacles for solid-state reaction route [32].

To obtain $LiFePO_4$ with small-size particle and high electronic conductivity by solid-state reaction route, organic acid, such as oxalic acid or citric acid, is used as carbon sources to prepare $LiFePO_4$/C composites. Organic acid can decompose into carbon which improve the electronic conductive of $LiFePO_4$, also the CO generated during decomposition and sintering works as a reducing agent avoiding oxidation of Fe(II). In addition, the organic acid can minimize particle size and make solid reactants touch closely [24, 33]. Kim et al. [33] have synthesized $LiFePO_4$ with good cycability by using oxalic acid as reducing agent. In the synthesis process of $LiFePO_4$/C, citric acid has not only effectively inhibited the grain growth, enabling the production of small size and well distribution of C in the $LiFePO_4$/C composite [23, 24] but also act as a surface-protecting agent, which increasing the necessary for improved Li-ion extraction [34]. Wang et al. [23] have synthesized $LiFePO_4$ using citric acid as raw material by low heating solid-state coordination method and microwave heating, and the results show that suitable amount of citric acid led to the formation of homogeneous nano-particles and improving performance of $LiFePO_4$. Yan et al. [35] report spheric $LiFePO_4$/C using proper addition of citric acid exhibit good performance at −20 °C. In addition, Liu et al. [36] confirm that citric acid is an effective carbon additive for improving electronic conductivity of $LiFePO_4$, and the $LiFePO_4$/C retains over 92% of its original discharge capacity beyond 2,400 cycles. Although $LiFePO_4$/C with small-size particle and high electronic conductivity have been synthesized by using oxalic acid or citric acid as carbon sources via solid-state reaction route, to the best of our knowledge, $LiFePO_4$/C material using two organic acids (oxalic acid and citric acid) as raw materials and its electrochemical performance at high temperature have not been reported until now.

Herein, we first employ oxalic acid and citric acid as chelating agent and carbon source, combine their advantageous to synthesis $LiFePO_4$/C nanocomposites via a simple solid-state reaction. The residual carbon in $LiFePO_4$/C nanocomposite from the decomposition of oxalic acid and citric acid can form a coating on the surfaces of the $LiFePO_4$ particles for electronic conduction. The as-prepared sample with oxalic acid and citric acid not only has smaller particle size (20–100 nm) and well-distribution but also exhibits large reversible rate capacity and excellent cycling stability under various current densities, especially at high temperature (60 °C). The impedance resistance of the as-prepared sample at different voltages and cycles were further investigated in detail.

Experimental

Preparation of the $LiFePO_4$/C composites

Stoichiometric Li_2CO_3, $(NH_4)_2HPO_4$, and $FeC_2O_4{\cdot}2H_2O$ were mixed and milled in an agate mortar with a pestle for 1 h to form a homogeneous fawn mixture. Adding different contents of oxalic acid (oxalic acid: Fe^{2+}=0.25:1, 0.5:1, 0.75:1, 1:1), the mixture were milled for another 1 h to yield the final precursors (precursors A, B, C, D). In a typical preparation, 2–5 g batches of the precursors were initially preheated to 350 °C for 3 h under flowing N_2. After cooling to room temperature, the precursors were milled again for about 0.5 h and finally annealed at 700 °C for 10 h to yield the $LiFePO_4$/C composites (samples A, B, C, D).

A modicum of citric acid (5% by mole ratio, corresponding to $LiFePO_4$) was mixed into precursor C, and the mixture was then milled for 0.5 h. After undergoing the same synthesis process, a $LiFePO_4$/C nanocomposite (sample E) was obtained.

Characterization

The crystalline phase of the resulting materials was analyzed by powder X-ray diffraction (XRD, MXP18AHF, MAC, Japan), which was carried out using Cu Kα radiation (λ=1.54056 Å). The grain size and morphology of the samples were observed using scanning electron microscope (SEM, JSM-6460A, Jeol, Japan) and transmission electron microscopy (TEM, H-600, Hitachi, Japan). The particle size distribution was measured with a Zeta Potential Analyzer (ELS-8000, Otsuka Electronics, Japan).

The electrodes which were tested at room temperature were made by dispersing 85% active materials, 10% acetylene black, and 5% poly(vinylidene fluoride) (by weight) in *N*-methyl pyrrolidinone solvent to form a homogeneous slurry, while the ones tested at 60 °C consisted of 80% active materials, 15% acetylene black, and 5% poly(vinylidene fluoride) (by weight) [37]. The slurry was then spread onto an aluminum foil substrate and dried at 120 °C for 10 h in a vacuum oven. The cells were assembled in an argon-filled glove box with lithium metal as the counter electrode, Celgard 2,400 as separator, and 1 mol L^{-1} $LiPF_6$ in a mixture of ethylene carbonate and dimethyl carbonate (EC: DMC= 1:1 by weight) as electrolyte. Galvanostatic charge and discharge cycling were performed between 2.5 and 4.1 V on a battery test instrument (CT2001A, Land, China) at selected temperatures. Cyclic voltammograms (CVs) were collected over a voltage range of 2.5 to 4.1 V at different scan rates using an electrochemical workstation (CHI660B, Chenhua, China). Electrochemical impedance spectroscopy (EIS) of the cells were conducted, and the spectra were recorded over the 0.1 to 100 kHz frequency range using an impedance

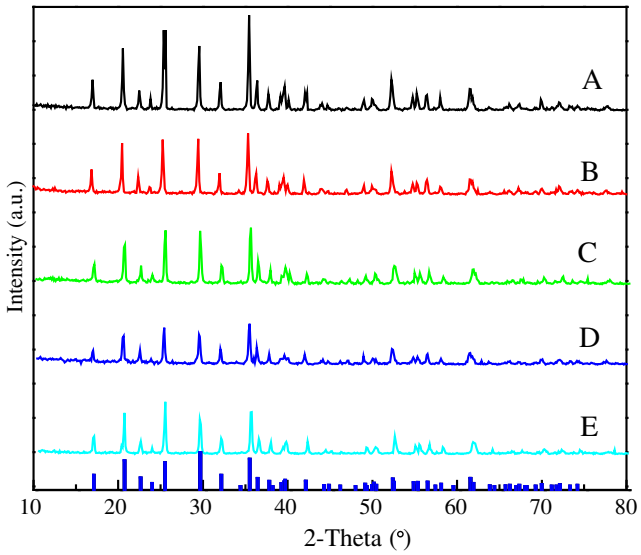

Fig. 1 X-ray diffraction patterns of the $LiFePO_4$/C nanocomposites (samples **a**–**e**)

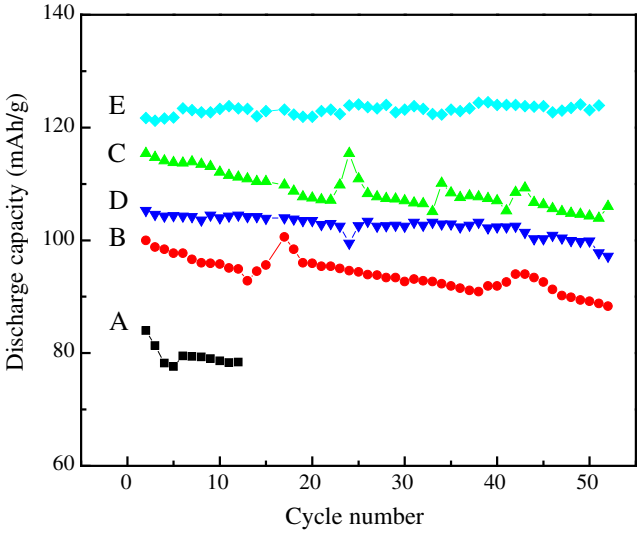

Fig. 3 Cycling performance of the $LiFePO_4$/C nanocomposites (samples **a**–**e**) at a current density of 170 mA/g (1 C rate)

measurement system (IM6e, Zahner, Germany), which applied a DC potential equal to the open circuit voltage of the cell and an ac oscillation of 5 mV.

Results and discussion

Figure 1 shows the XRD patterns of the $LiFePO_4$/C nanocomposites (samples A, B, C, D, and E). It can be observed that the positions of the characteristic peaks of the samples are almost the same as those of single-phase pure, ordered, orthorhombic, olivine-structured $LiFePO_4$. The intensity of the peaks of the samples is reduced with ratio of oxalic acid: Fe^{2+} from 0.25:1 to 1:1, suggesting the relatively poor crystalline of carbon-coated $LiFePO_4$. However, no carbon peaks are detected due to its low content and amorphous state [38].

The SEM of $LiFePO_4$/C (sample C and E) is used to evaluate the effect of citric acid on the surface morphology.

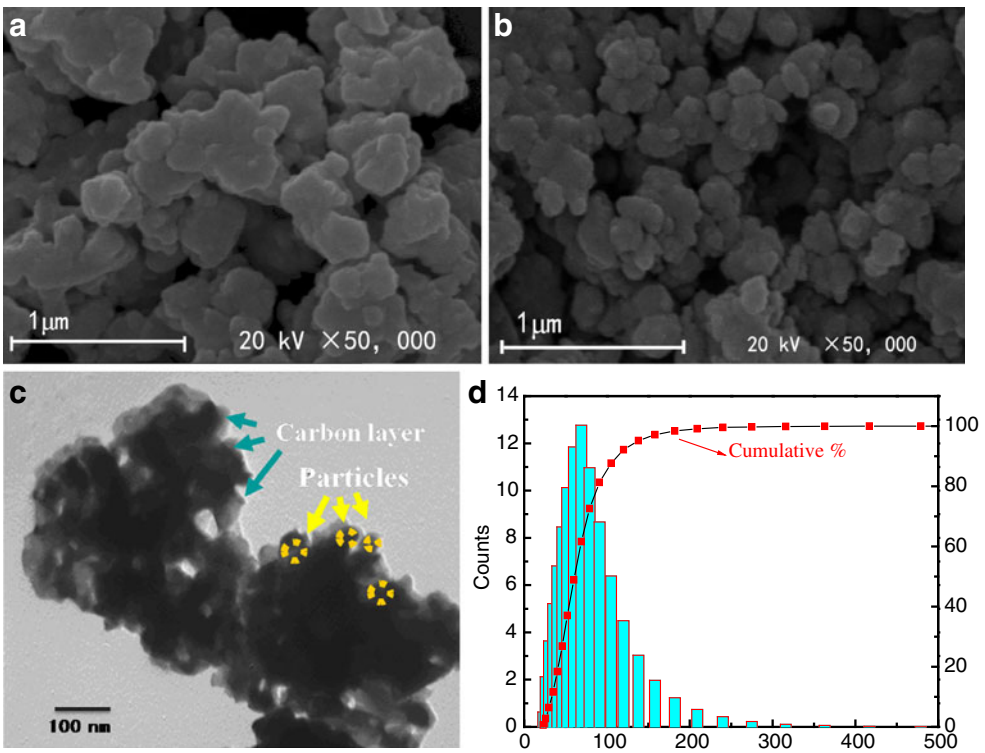

Fig. 2 SEM images of $LiFePO_4$/C (**a** sample C; **b** sample E), TEM image (**c** sample E) and particle size distribution pattern of $LiFePO_4$/C (**d** sample E)

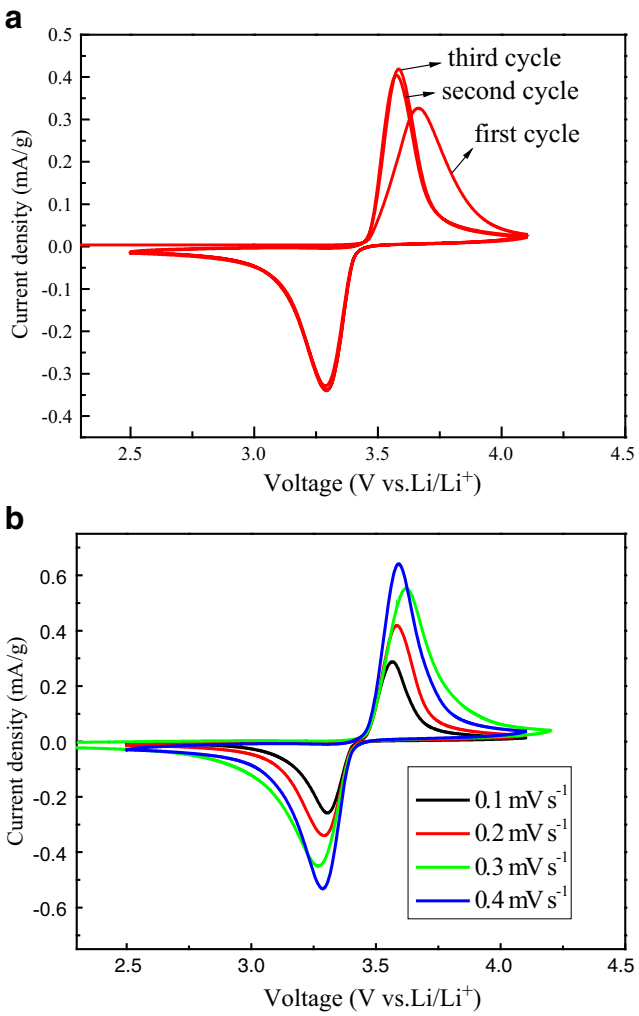

Fig. 4 Cyclic voltammograms of $LiFePO_4$/C nanocomposite (sample E): **a** the first 3 cycles at a scan rate of 0.2 mV/s; **b** the second cycle at different scan rates

It can be observed from Fig. 2(a, b) that the $LiFePO_4$ particles (sample E) are smaller, well distribution and more uniform after adding citric acid, which indicating that a small amount of citric acid has inhibited the grain growth. Figure 2(c) presents TEM image of sample E. It can be seen that the nanocomposite is composed of many small particles, which are completely coated by carbon film to form the carbon-coated structure. The sizes of these particles are clearly reflected in the particle size distribution pattern (Fig. 2(d)). It can be seen that approximately 80% of the $LiFePO_4$/C particles are in range of 20–100 nm, with an average particle size of ~60 nm. The formation of homogeneous nanosized particles might be ascribed to citric acid addition: the added citric acid expanded after being heated, thus reducing the surface tension of the precursors and inhibiting the grain growth. The small particle size and carbon-coated structure can efficiently shorten the diffusion length of Li^+ and enhance the electric conductivity of the electrode [39–41]. In view of the differences at morphology and particles size, sample E is anticipated to exhibit superiority electrochemical performance.

Figure 3 shows the cycling performance of the $LiFePO_4$/C nanocomposites (samples A, B, C, D, and E) at a constant current density of 170 mAh/g (1 C rate). Among the cycling performance curves of the samples A, B, C, and D, progressive enhancement of the discharge capacity becomes obvious with increasing amounts of oxalic acid. When the amount of oxalic acid rises to 0.75 (sample C), the material possesses the best electrochemical performance: The initial discharge capacity is the highest (115.4 mAh/g), and the cycling performance is the steadiest among the four samples (samples A, B, C, and D). The results indicate that the oxalic acid content should have a great influence on the performance of $LiFePO_4$ and needs to be optimized. Compared with the cycling performance of sample C, sample E (the material with citric acid) has

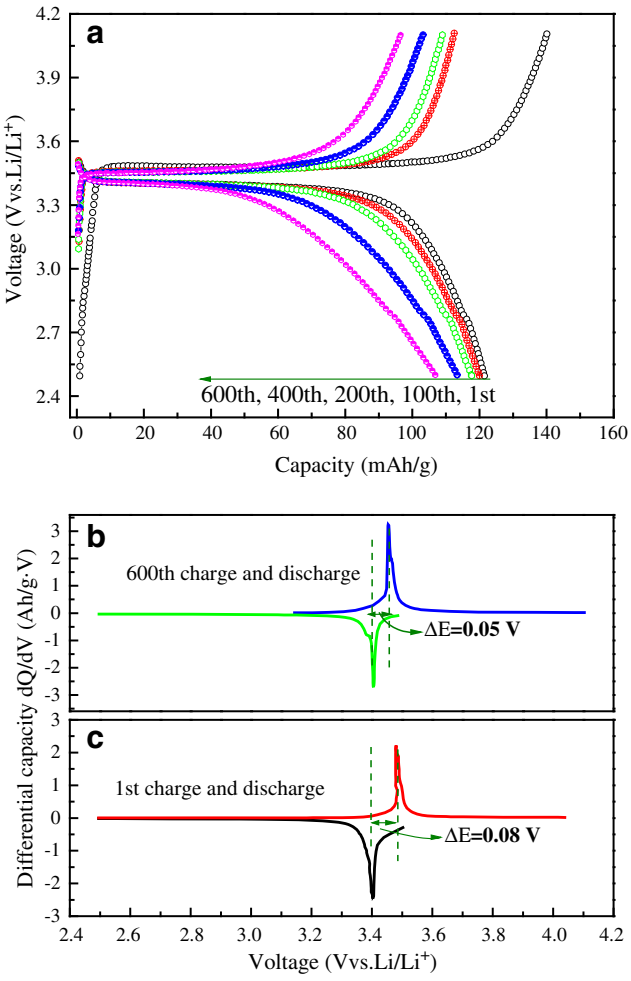

Fig. 5 **a** Galvanstatic charge/discharge profiles of $LiFePO_4$/C nanocomposite (sample E) at the 1 C rate during long cycling; **b** 600th charge/discharge, and **c** 1st charge/discharge differential capacity, dQ/dV (Ah/g·V), based on plots extracted from (**a**)

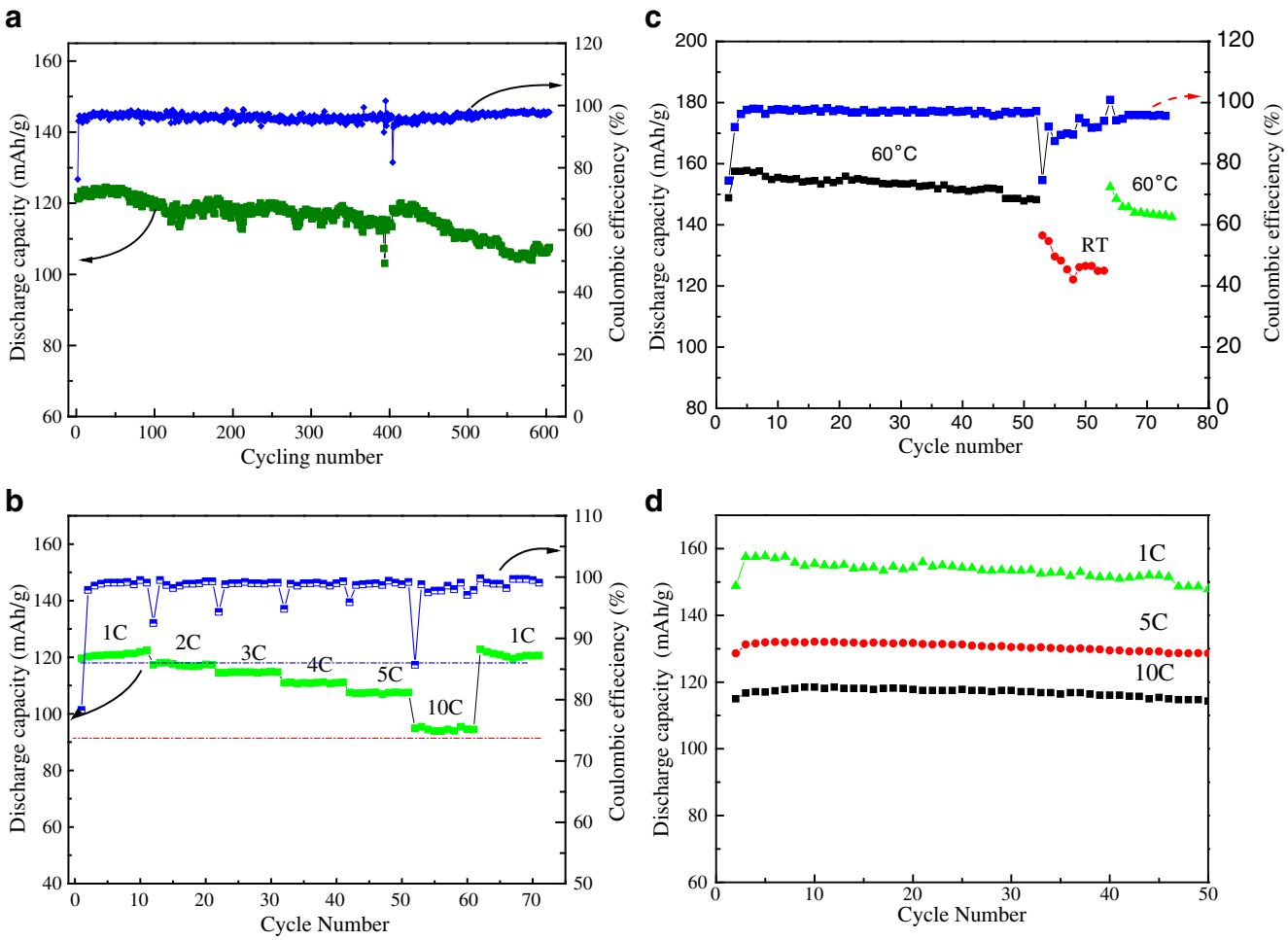

Fig. 6 Cycling performance of $LiFePO_4$/C nanocomposite (sample E): **a** at 1 C rate, **b** at various charge/discharge rates during continuous cycling, **c** at different temperatures during continuous cycling at 1 C, and **d** at various charge/discharge rates at 60 °C

higher initial discharge capacity and better cycling performance, indicating that citric acid can play an important role in improving the discharge capacity and cycling performance of $LiFePO_4$/C nanocomposites, which is consistent with the results of SEM.

To analyze the electrochemical properties of the $LiFePO_4$/C nanocomposite (sample E), cyclic voltammograms are collected, as shown in Fig. 4. The voltage is in the range of 2.5 to 4.2 V vs. Li/Li^+. Figure 4(a) shows the first 3 cycles at a scan rate of 0.2 mV/s. There are only a single pair of peaks for each cycle, implying the typical two-phase reaction between $LiFePO_4$ and $FePO_4$ [4]. The redox peaks of the first cycle are located at 3.25 and 3.66 V, which corresponds to the extraction and insertion of Li^+. After "activation" by the first redox, the current peaks of the following cycles become sharper and larger. The curves of the second and the third cycles are in good superposition, indicating that the electrochemical reversibility of $LiFePO_4$/C nanocomposite (sample E) is established after the first cycle [32]. Figure 4(b) shows cyclic voltammograms of the second cycle of $LiFePO_4$/C nanocomposite (sample E) at different scan rates. With enhancement of the scan rate, the redox peaks of $LiFePO_4$/C nanocomposite (sample E) are still symmetric, revealing that $LiFePO_4$/C nanocomposite (sample E) possesses excellent reversibility of the redox reaction at various scan rates.

Figure 5(a) shows the galvanstatic charge/discharge profiles of $LiFePO_4$/C nanocomposite (sample E) at 1 C rate over 600 cycles. The charge profiles have flat voltage plateaus around 3.5 V while that of the discharge profiles is around 3.4 V. The flat voltage profile areas and the decrease in the discharge capacity with cycling are due to the decreasing amounts of utilizable activated material [42]. The differences (ΔE) between the charge and discharge voltage are clearly shown in 5(b) and (c). The difference (ΔE) is 0.08 V for the 1st cycle and 0.05 V for the 600th cycle, respectively. The declining trend of ΔE demonstrates that the voltage polarization of the material during long-term cycling is comparatively small, which should be ascribed to the high electronic conductivity. This may be

affected by the improvement in the kinetics of the lithium intercalaction/deintercalaction at the electrode/electrolyte interface and/or the high conductivity through the carbon film on the $LiFePO_4$/C [43, 44].

Good cycling performance is a remarkable advantage of the $LiFePO_4$/C nanocomposite (sample E). Figure 6(a) shows the cycling performance of the $LiFePO_4$/C nanocomposite (sample E) at 1 C rate. The discharge capacity is 121.7 mAh/g for the 1st cycle, increases up to 124.5 mAh/g in the following 50 cycles, and remains constant up to 500 cycles. Over the 500 cycles, the capacity fading per cycle is 0.12%, and the Coulombic efficiency >96%, which indicates that the $LiFePO_4$/C nanocomposite (sample E) possesses excellent cycling performance at the 1 C rate.

The high-rate capability is another remarkable advantage for the $LiFePO_4$/C nanocomposite (sample E). The discharge capacity of the $LiFePO_4$/C nanocomposite (sample E) varies with different charge/discharge currents, as shown in Fig. 6(b). This material is capable of delivering 120.2, 117.3, 114.5, 110.9, 107.5, and 94.9 mAh/g at the rates of 1 , 2 , 3 , 4 , 5 , and 10 C, respectively. Although the discharge capacities decrease regularly with increasing current rate, they can be fully regained once the charge/discharge current returns to the 1 C rate. Compared with the initial discharge capacity of 120.2 mAh/g, a higher discharge capacity of 122.8 mAh/g is obtained when the discharge current rate return to 1 C rate, which makes it clearly that the $LiFePO_4$/C nanocomposite (sample E) possesses admirable electrochemical reversibility and a stable structure at various charge/discharge currents. The excellent electrochemical performances are ascribing to small, uniform distribution and close contact with each other of the particles.

The effects of the testing temperature on the electrochemical characteristics of $LiFePO_4$/C nanocomposite (sample E) were investigated with different charge/discharge rates. Figure 6(c) shows the cycling performance of $LiFePO_4$/C nanocomposite (sample E) at different temperatures (at room temperature and 60 °C) with the 1 C rate. The average discharge capacity is 153.2 mAh/g at 60 °C for the first 50 cycles, which is higher than the corresponding average discharge of 127.8 mAh/g at room temperature in the subsequently 10 cycles. When the testing temperature return to 60 °C after 60 cycles, the $LiFePO_4$/C nanocomposite (sample E) can still deliver a discharge capacity of 152.3 mAh/g.

The high-rate cycling performance of the material at 60 °C is perfect. The initial discharge capacity at 60 °C is 153 mAh/g at 1 C, 128.6 mAh/g at 5 C, and 115 mAh/g at 10 C (as shown in Fig. 6(d)), and there are little capacity loss up to 50 cycles for each of them. The excellent cycling performances at high rate at selected temperatures are due to the enhancement of electrical conductivity by the carbon film on the surfaces of the $LiFePO_4$/C.

The kinetic processes of the $LiFePO_4$/C nanocomposite (sample E) can be clearly depicted by EIS measurements. Here, impedance measurements were carried out at room temperature on cells at selected voltages of $LiFePO_4$/C versus Li in the voltage range of 2.0 to 4.1 V during the initial charge cycle, as shown in Fig. 7(a). The intercept at the Z_{re} axis in high frequency corresponds to the Ohmic resistance (R_e), which represents the total electric resistance of the electrode materials, the electrolyte resistance, and the resistance of the electric leads [45]. The semicircle in the middle frequency range indicates the charge transfer resistance (R_{ct}). The inclined line in the low frequency range is attributed to the Warburg impedance (Z_w), which is associated with lithium-ion diffusion in the $LiFePO_4$ particles [46]. The charge transfer resistance (R_{ct}) is about 400 Ω for the fresh cell, rises to 650 Ω when the charge voltage is 3.2 V and then descends progressively to about

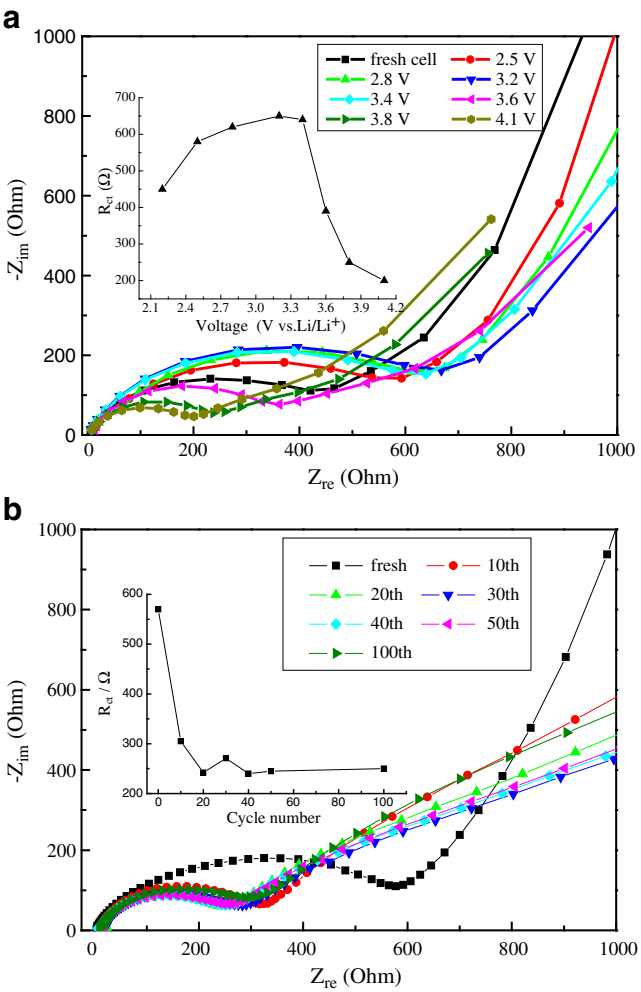

Fig. 7 Nyquist plots for the $LiFePO_4$/C nanocomposite (sample E) electrode **a** at various voltages during the initial charge cycle, and **b** after 10, 20, 30, 40, 50, and 100 cycles at the 1 C rate. The insets show the charge transfer resistance at different voltages (**a**) and different cycle numbers (**b**)

250 Ω after the charge voltage changes from 3.4 to 4.1 V. The change in the R_{ct} is clearly shown in the inset of 7(a). The change in R_{ct} before 3.2 V would have a close relationship to the appearance of the $FePO_4$ phase and high lithium ion concentrations in the electrolyte. The R_{ct} is the highest when $FePO_4$ is the major phase in the charge state. Wang [47] et al. have reported that the R_{ct} is much bigger at higher lithium ion concentrations in the electrolyte than at lower ones. After the cell is charged at 3.4 V, especially at 4.1 V, the lithium ion concentrations are lower, and the $LiFePO_4$/C cathode material has been completely activated, which can contribute to the decline of the charge transfer resistance values. Figure 7(b) shows impedance spectra for the $LiFePO_4$/C nanocomposite (sample E) in the open circuit state after different cycling tests at the 1 C rate. Obviously, the R_{ct} of the $LiFePO_4$/C electrode is smaller after the 1st cycle for the fresh electrode, but there are no obvious changes in extended cycling tests (as shown in the inset of Fig. 7(b)), which are consistent with the CVs. The similar impedance spectra of the $LiFePO_4$/C after the 1st cycle appear to be due to the better electrical contact and the improvement of the intrinsic electrical conductivity by the carbon film on the $LiFePO_4$ particles. These results indicate that the kinetic behavior of the $LiFePO_4$/C nanocomposite is stable and imply superior cyclability of the material.

The excellent performances of the $LiFePO_4$/C nanocomposite (sample E) obtained in our work can be ascribed to the ordered olivine structure of $LiFePO_4$, along with the unique microstructure, small particles, and high conductivity improved by the carbon film, which can make possible a near approach to the large-scale use of $LiFePO_4$ as a cathode material for high-energy-density, high-power lithium-ion batteries in electric vehicles, and other mobile devices.

Conclusion

The superior electrochemical performance of $LiFePO_4$/C nanocomposite at high rate and over long cycling was achieved by a simple solid-state reaction by using oxalic acid and citric acid as chelating agent and carbon source. The residual carbon can coat the surfaces of the $LiFePO_4$ particles to form a carbon-coated structure, which can improve the electronic conductivity of $LiFePO_4$. The $LiFePO_4$/C nanocomposite with citric acid (sample E) delivers discharge capacities of 123.1 mAh/g at 1 C at room temperature, 153.0 mAh/g at 1 C at 60 °C, 128.6 mAh/g at 5 C at 60 °C, and 115.0 mAh/g at 10 C at 60 °C, respectively. During long-term cycling at different rates, the discharge capacity has no noticeable fading. The electrochemical performance and the simple preparation route of the $LiFePO_4$/C nanocomposite for lithium-ion batteries reported here demonstrate its promising application in vehicles and other mobile devices.

Acknowledgements This work was supported by the Nature Science Foundation of Xinjiang Province (Grant Nos. 200821121 and 200821122), the National Natural Science Foundation of China (Grant Nos. 20866009 and 20861008), Technological People Service Corporation (2009GJG40028), and the Science and technology Foundation of Urumqi (y08231006).

References

1. Whittingham MS (2004) Chem Rev 104:4271
2. Peterson SB, Apt J, Whitacre JF (2010) J Power Sources 195:2385
3. Masarapu C, Subramanian V, Zhu HW, Wei BQ (2009) Adv Funct Mater 19:1
4. Padhi AK, Nanjundaswamy KS, Goodenough JB (1997) J Electrochem Soc 144:1188
5. Sun YK, Myung ST, Park BC, Prakash J, Belharouak L, Amine K (2009) Nat Mater 8:320
6. Li D, Huang YD, Jia DZ, Guo ZP, Bao SJ (2010) J Solid State Electr 14:889
7. Yu DYW, Fietzek C, Weydanz W, Donoue K, Inoue T, Kurokawa H, Fujitani S (2007) J Electrochem Soc 154:A253
8. Wang YG, Wang YR, Hosono E, Wang KX, Zhou HS (2008) Angew Chem Int Ed 47:1
9. Konarova M, Taniguchi I (2010) J Power Sources 195:3361
10. Lin Y, Gao MX, Zhu D, Liu YF, Pan HG (2008) J Power Sources 184:444
11. Herle PS, Ellis B, Coombs N, Nazar LF (2004) Nat Mater 3:147
12. Meethong N, Kao YH, Speakman SA, Chiang YM (2009) Adv Funct Mater 19:1060
13. Yamada A, Kudo Y, Liu KY (2001) J Electrochem Soc 148: A1153
14. Gao F, Tang ZY, Xue JJ (2007) Electrochim Acta 53:1939
15. Zheng JC, Li XH, Wang ZX, Guo HJ, Zhou S (2008) J Power Sources 184:574
16. Kang B, Ceder G (2009) Nature 458:190
17. Xie HM, Wang RH, Ying JR, Zhang LY, Jabout AF, Yu HY, Yang GL, Pan XM, Su ZM (2006) Adv Mater 18:2609
18. Amin R, Lin C, Peng JB, Weichert K, Acarturk T, Starke U, Maier J (2009) Adv Funct Mater 19:1697
19. Hu YQ, Doeff MM, Kostecki R, Fiñones R (2004) J Electrochem Soc 151:A1279
20. Kim JK, Chauhan GS, Ahn JH, Ahn HJ (2009) J Power Sources 189:391
21. Li LJ, Li XH, Wang ZX, Wu L, Zheng JC, Guo HJ (2009) J Phys Chem Solids 70:238
22. Arnold G, Garche J, Hemmer R, Ströbele S, Vogler C, Wohlfahrt-Mehrens M (2003) J Power Sources 119–121:247
23. Wang L, Huang YD, Jiang RR, Jia DZ (2007) Electrochim Acta 52:6778
24. Hao YJ, Lai QY, Liu DQ, Xu ZU, Ji XY (2005) Mater Chem Phys 94:382
25. Zhang Y, Feng H, Wu XB, Wang LZ, Zhang AQ, Xia TC, Dong HC, Liu MH (2009) Electrochim Acta 54:3206
26. Ellis B, Kan WH, Makahnouk WRM, Nazar LF (2007) J Mater Chem 17:3248
27. Wang ZL, Ching SR, Wen CY, Chen Y, Xia DG (2008) J Power Sources 184:633

28. Teng F, Santhanagopalan S, Lemmens R, Geng XB, Patel P, Meng DD (2010) Solid State Sci 12:952
29. Liu HP, Wang ZX, Li XH, Guo HJ, Peng WJ, Zhang YH, Hu QY (2008) J Power Sources 184:469
30. Zhu BQ, Li XH, Wang ZX, Guo HJ (2006) Mater Chem Phys 98:373
31. Teng TH, Yang MR, Wu SH, Chiang YP (2007) Solid State Commun 142:389
32. Wang YQ, Wang JL, Yang J, Nuli Y (2006) Adv Funct Mater 16:2135
33. Kim K, Cho YH, Kam D, Kim HS, Lee JW (2010) J Alloys Compd 504:166–170
34. Landschoot NV, Kelder EM, Schoonman J (2004) Solid State Ionics 166:307–316
35. Yan XD, Yang GL, Liu J, Ge YC, Xie HM, Pan XM, Wang RS (2009) Electrochim Acta 54:5770
36. Liu J, Wang JW, Yan XD, Zhang XF, Yang GL, Jalbout AF, Wang RS (2009) Electrochim Acta 54:5656
37. Maccario M, Croguennec L, Le CF, Delmas C (2008) J Power Sources 183:411
38. Liu YY, Cao CB, Li J (2010) Electrochim Acta 55:3921
39. Lee SB, Cho SH, Cho SJ, Park GJ, Park SH, Lee YS (2008) Electrochem Commun 10:1219
40. Chen JJ, Whittingham S (2006) Electrochem Commun 8:855
41. Rui XH, Li C, Chen CH (2009) Electrochim Acta 54:3374
42. Andersson AS, Thomas JO (2001) J Power Sources 97–98: 498
43. Jin B, Gu HB, Zhang WX, Park KH, Sun GP (2008) J Solid State Electrochem 12:1549
44. Chung SY, Bplomg J, Chiang YM (2002) Nat Mater 1:123
45. Gao F, Tang ZY (2008) Electrochim Acta 53:5071
46. Shin HC, Cho WI, Jang H (2006) Electrochim Acta 52:1472
47. Wang Q, Evans N, Zakeeruddin SM, Exnar I, Gratzel M (2007) J Am Ceram Soc 129:3163